Journal of Catalysis 275 (2010) 170–180

Contents lists available at ScienceDirect

Journal of Catalysis

journal homepage: www.elsevier.com/locate/jcat

Methanol to hydrocarbons over large cavity zeolites: Toward a unified description of catalyst deactivation and the reaction mechanism

Morten Bjørgen [a,*], Sema Akyalcin [b], Unni Olsbye [c], Sandrine Benard [c], Stein Kolboe [c], Stian Svelle [c,**]

[a] Norwegian University of Science and Technology, Department of Chemistry, N-7491 Trondheim, Norway
[b] Anadolu University, Department of Chemical Engineering, 26555 Eskisehir, Turkey
[c] inGAP Center of Research Based Innovation/Center for Materials Science and Nanotechnology (SMN), University of Oslo, Department of Chemistry, N-0315 Oslo, Norway

ARTICLE INFO

Article history:
Received 17 March 2010
Revised 21 July 2010
Accepted 1 August 2010

Keywords:
MTH
MTO
MTG
H-beta
H-MCM-22
H-mordenite
Isotopic labeling
Reaction mechanism

ABSTRACT

The reaction mechanism for the conversion of methanol to hydrocarbons over three large cavity zeolites, H-beta, H-MCM-22, and H-mordenite, has been investigated. ^{13}C methanol was co-reacted with ^{12}C benzene to study the buildup and further reactions of the intermediates formed. Co-reaction was required, as these aromatic intermediates will not be formed from pure methanol at temperatures low enough to actually monitor these events. The reactions were followed by dissolving quenched catalysts in HF followed by extraction of the organic compounds and analysis by GC–MS. The same hydrocarbon compounds are formed inside the pores of three zeolites, and it is the most substituted methylbenzenes that function as reaction intermediates in the hydrocarbon pool mechanism for the conversion of methanol. The heptamethylbenzenium cation was for the first time detected and shown to serve as a key reaction intermediate in zeolite catalysts other than H-beta. The formation of bicyclic coke precursors was also investigated, and progress has been made toward a more complete description of the reactions leading to catalyst deactivation. Quantum chemical calculations have shed light on the processes leading to coke precursors. The profound similarities between H-beta, H-mordenite, and H-MCM-22 shown herein constitute a significant step toward a unified understanding of the MTH reaction over acidic zeolites.

1. Introduction

During the last two decades, substantial advances in the fundamental understanding of the reaction mechanism of the methanol-to-hydrocarbons reaction have been made [1,2]. A major breakthrough was the proposal of the hydrocarbon pool mechanism by Dahl and Kolboe [3,4]. It now seems clear that multiple methylated aromatics play key roles in this mechanism proposal. These species are frequently referred to as hydrocarbon pool species. In particular, the highest substituted congeners, i.e. hexamethylbenzene (hexaMB) and its further methylation product, the heptamethylbenzenium cation (heptaMB$^+$), have been proved to be the main constituents of the hydrocarbon pool in the spacious H-SAPO-34 [5–8] and H-beta [9–11] catalysts, respectively. It is believed that alkenes in the C_2–C_4 range may be split off from these species in a series of complex rearrangement and dealkylation reactions with concomitant formation of less substituted homologs. This monomolecular mode of alkene formation from the hydrocarbon pool species is known as the *paring route* [12–14]. Alternatively, a cationic methylbenzenium species (e.g. heptaMB$^+$) may be deprotonated resulting in formation of an exocyclic double bond, such as seen in hexamethylmethylenecyclohexadiene (HMMC), see Scheme 1. Methylations of this exocyclic double bond will lead to alkyl side chains on the benzene ring, which can be eliminated as an alkene. This is referred to as the *side-chain methylation route* [15–17].

The initial studies of the hydrocarbon pool mechanism and the reactivity of the highly methylated aromatics were conducted on the H-SAPO-34 catalyst. HexaMB, once formed from methanol within the H-SAPO-34, cages were found to be highly reactive, decomposing into alkenes and lower methylbenzenes [5,6,18]. Further insights were reached when hexaMB was reacted alone over the H-beta zeolite [9,17]. Again, hexaMB was found to be highly reactive, and the products formed were closely similar to those obtained with a methanol feedstock. Another step forward was made using isotopic labeling. ^{12}C benzene and ^{13}C methanol were co-reacted at low temperatures over H-beta [10]. At the very lowest reaction temperatures (210 °C), HMMC, which resides in the zeolite in its protonated form as heptaMB$^+$, was unequivocally identified. HMMC/heptaMB$^+$ was shown to be unstable upon heating and could hardly be observed above 300 °C. Moreover, using isotopic labeling, the formation of alkenes from HMMC/heptaMB$^+$ was found to be in accord with the paring route [10]. Subsequently, the high relevance of heptaMB$^+$ as a hydrocarbon pool species was

* Corresponding author. Fax: +47 73 55 08 77.
** Corresponding author. Fax: +47 22 85 54 41.
E-mail addresses: morten.bjorgen@chem.ntnu.no (M. Bjørgen), stian.svelle@kjemi.uio.no (S. Svelle).

0021-9517/$ - see front matter © 2010 Elsevier Inc. All rights reserved.
doi:10.1016/j.jcat.2010.08.001

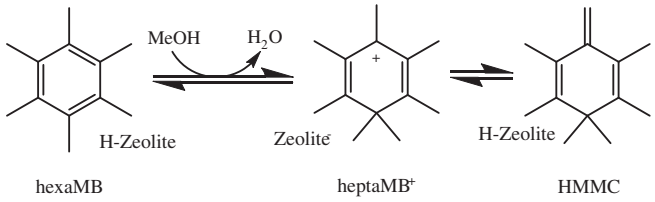

Scheme 1. Methylation of hexaMB leads to formation of the heptaMB + cation, which may be deprotonated to yield a compound with an exocyclic double bond, HMMC.

confirmed directly by reacting HMMC over H-beta [11]. Hence, a large amount of research, carried out independently by two groups, point to the higher methylbenzenes as intermediates in the alkene-forming reaction. However, the bulk of these results have been obtained for the H-SAPO-34 and the H-beta catalysts.

Recently, the MTH reaction mechanism in H-ZSM-5 has been examined carefully, and it was found that, in contrast to H-SAPO-34 and H-beta, it is predominantly the lower methylbenzenes that are active intermediates [19–23]. Moreover, alkene formation through repeated methylation and cracking of the C_{3+} alkenes is particularly important in H-ZSM-5 [21,24]. In this report, we investigate the general validity of the idea that it is the highest methylbenzenes that are the most important reaction intermediates in spacious, large pore zeotype materials by examining a wider range of such catalysts, that is, H-mordenite and H-MCM-22. The experiments discussed in the present contribution are particularly focused toward examining the reactivity of aromatic species confined within the catalyst pores. Whether or not additional product formation mediated by alkene methylation and ensuing cracking steps takes place is not explicitly evaluated.

Benzene and methanol have been co-reacted at a wide range of temperatures in order to study the buildup and reactivity of the relevant methylbenzene intermediates, which would otherwise not be formed from pure methanol at temperatures low enough to actually monitor them. Also, by using ^{13}C labeled methanol, it is possible to distinguish between ring- and methyl carbons in the methylbenzenes.

2. Experimental

A description of the procedure for calculating the $^{12}C/^{13}C$ isotopic content and distribution based on GC–MS analyses have been given previously and will not, for the sake of brevity, be repeated here [3,25].

2.1. Catalysts

Three large cavity zeolite samples have been investigated: H-beta (Si/Al = 12), H-MCM-22 (Si/Al = 11), and H-mordenite (Si/Al = 22). The H-mordenite and H-beta catalysts were commercially available from Süd Chemie and P.Q. Zeolites B.V., respectively. H-MCM-22 was synthesized in-house according to the procedure reported by Güray et al. [26].

2.2. Catalyst characterization

Experimental details on the catalyst characterization by ICP-AES and acidity measurements by FT-IR have been described previously [27]. Capillary X-ray diffractograms were recorded on a Siemens D5000 instrument in transmission Debye–Scherrer geometry using Cu Kα1 radiation. Scanning electron micrographs were collected on a FEI Quanta 200 FEG–ESEM equipped with an Everhart–Thornley detector. An accelerating voltage of 10 kV was used. N_2 adsorption isotherms were measured using a Belsorp-mini II instrument at −196 °C. The samples were outgassed in vacuum for 5 h at 300 °C, and the total surface area was determined by the BET method, based on p/p_0 data in the range of 0.01–0.15.

2.3. Catalytic testing

Experimental details on the catalytic testing and the gas chromatography have been described previously [9,10,28]. The experiments were carried out in a fixed bed microreactor at 225–350 °C, using 40 mg catalyst. Methanol, either ^{13}C enriched (Cambridge Isotope Laboratories, 99% ^{13}C) or ordinary ^{12}C methanol (BDH Laboratory Supplies, >99.8%), and benzene (Riedel–deHaën, >99.5%) were fed by simultaneously passing separate nitrogen carrier gas streams through saturation evaporators kept at 0 °C. The carrier gas flow was maintained at 5 mL/min for benzene and at 31 mL/min for methanol. The two saturated gas streams were mixed and led to the reactor. Resulting feed partial pressures were 5 and 34 mbar for benzene and methanol, respectively, corresponding to feed rates (WHSV) of 0.9 and 2.5 h^{-1}. This results in a molar methanol:benzene ratio of 7:1 and a H:C ratio of ∼1.5 in the feed when water formation is taken into account, which is somewhat lower than for a neat methanol feedstock (H:C ratio of 2). The effluent was analyzed by online GC–FID after 60 s of co-reaction at a reaction temperature of 350 °C.

2.4. Analyses of the retained hydrocarbons by dissolution in HF and extraction

The protocol employed is based on previous procedures [5,29,30]. Briefly, after 90 s of reaction, the catalyst was rapidly cooled, transferred to a screw cap Teflon tube, and dissolved in hydrofluoric acid (33 mg catalyst in 1 mL 15% HF). Thereafter, the organic material residing in the pores thus liberated were extracted by CCl_4 (1 mL, with C_2Cl_6 as internal standard), and the extract analyzed by GC–MS.

2.5. Quantum chemical calculations

The thermodynamic feasibility of the methylation of the methylnaphthalenes was investigated by quantum chemical calculations performed with the Gaussian03 program [31]. Two types of calculations were carried out. First, structure optimization of the hydrocarbons were carried out at the B3LYP/6–31G** level of theory. Due to the large number of methyl groups on many of these species, special care was needed to ensure that there were no negative eigenvalues in the resulting Hessian, i.e. the true energy minimum was found. Thereafter, more accurate thermochemical data were calculated using the composite G3MP2B3 method [32]. The G3MP2B3 method yields an average absolute deviation of 5.2 kJ/mol for the 299 energies (enthalpies of formation, ionization potentials, electron affinities, proton affinities) of the G2/97 test set [32]. All methylnaphthalene (MN) isomers (from naphthalene to octaMN, 76 in total) and several dihydrotetraMN (15) and dihydropentaMN isomers (6) were investigated.

3. Results

3.1. Description of catalyst topologies

The salient features of the three topologies are shown in Figs. S.1–S.3 of Supplementary material.

The beta zeolite (Fig. S.1) is a disordered structure consisting of three intergrown polymorphs, denoted A, B, and C [33,34]. All three polymorphs have a three-dimensional 12-ring channel system. The polymorphs are individually ordered, but the stacking results in

disorder along the *c*-axis. For all the polymorphs, two channel systems are linear and topologically identical. They are mutually orthogonal and perpendicular to the *c*-axis. These two sets of channels intersect and form a third channel system that is sinusoidal and parallel to the *c*-axis. Polymorph A has a tetragonal framework. Polymorphs B and C both have monoclinic symmetry. The linear channels of polymorph A have the dimensions 6.6 × 7.7 Å, and the tortuous channel is smaller, 5.6 × 5.6 Å [35].

MCM-22 (Fig. S.2) has a rather peculiar framework structure that comprises two independent, non-intersecting pore systems, both accessible through 10-membered rings. One of them is composed of two-dimensional sinusoidal 10-membered rings (apertures 5.5 × 4.0 and 5.1 × 4.1 Å [35]), and the other consists of large cages with inner diameter 7.1 Å, delimited by 12-membered rings. The pore networks of MCM-22 have unusual characteristics, often resulting in catalytic behavior not expected for medium-pore zeolites as MCM-22 often shows properties similar to those of 12-ring zeolites [36]. As revealed by Lawton et al. [37], external zeolitic pockets (each of these is half of a cage) cover the surface of the crystals and may influence the catalytic properties of this material.

The mordenite structure (Fig. S.3) has 12- and eight-membered ring channels that run parallel to the *c*-axis. These systems are connected by eight-ring channels parallel to the *b*-axis. Typical channel dimensions are 6.5 × 7.0 and 5.7 × 2.6 Å for the 12- and eight-membered rings, respectively [35]. These flattened eight rings are in practice not accessible to any diffusing species. The perpendicular eight-ring channels that run in the *b*-direction are highly tortuous, leading to a very narrow region that effectively functions as a diffusion barrier and leads to the so-called side-pockets to the 12 rings. Thus, the possibility for most molecules to pass through these eight rings is severely sterically hindered, and the mordenite structure is thus in practice a one-dimensional 12-ring system.

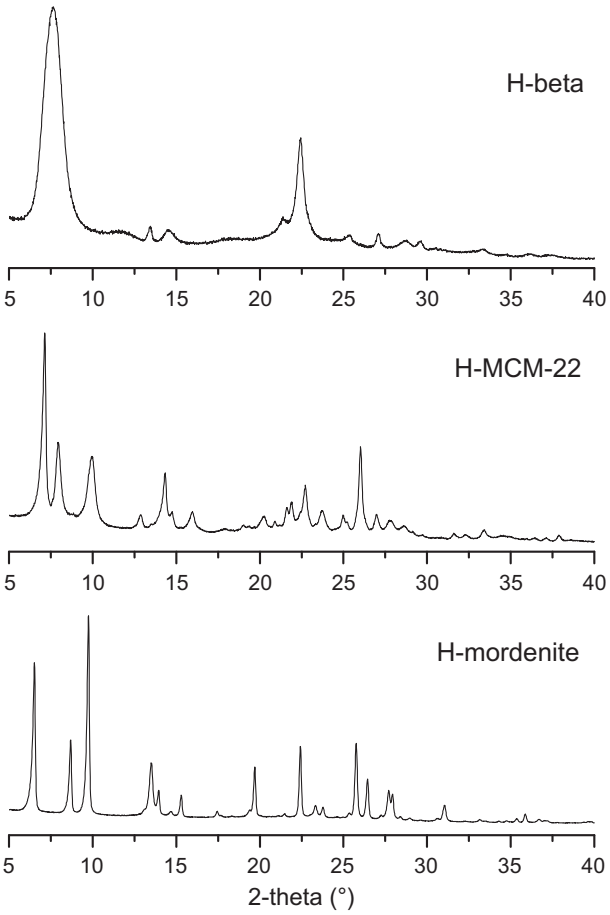

Fig. 1. Powder X-ray diffractograms of the three catalysts.

3.2. Catalyst characterization

The samples employed in this study have been characterized previously [27]. Briefly, the compositions were determined using ICP-AES, and the Si/Al ratios were 12 for H-beta, 11 for H-MCM-22 and 22 for H-mordenite. FT-IR combined with adsorption of CO was used to probe the acidic sites, and it was found that there are no significant differences in the acid strengths of the three catalysts. Also, it was found that all three catalysts contain similar amounts of Lewis acidic sites.

X-ray diffractograms for the three catalyst samples are shown in Fig. 1, and they confirm that the samples are highly crystalline materials of the expected phase. The peaks in the H-beta diffractogram are especially wide. This is caused by the fact that H-beta is a disordered intergrowth of three polymorphs and that this particular sample consists of very small crystals, leading to peak broadening.

The BET surface areas were determined to be 663 m^2/g for H-beta, 469 m^2/g for H-MCM-22 and 449 m^2/g for H-mordenite. These values are within those previously reported for these materials [38,39].

SEM micrographs of H-MCM-22 and H-mordenite are given in Fig. 2. The H-beta sample consists of small crystals in the range 0.1–0.7 μm according to the producer and was not amenable to analysis by SEM. The small crystal size is reflected by the broad peaks in the diffractograms. The H-MCM-22 sample (Fig. 2, left panel) has a complex morphology. The major part of the sample appears to consist of particles with a diameter of ~5 μm. Narrow needles are seen dispersed among the larger particles. Upon closer inspection (see inset), it appears that the ~5-μm particles have some surface fine structure and might to some extent be composed of intergrown, bundled needles. The H-mordenite (Fig. 2, right panel) sample was not easily characterized by SEM, due to unusually ill-defined crystals. The quite narrow peaks in the diffractograms indicate crystals larger than those of the H-beta sample. In the overview image, some larger chunks of diameter about 5 μm are seen; these could be agglomerates. The inset shows that the remainder of the sample consists of chips or grains with diameter slightly below 1 μm.

3.3. Analyses of the gas-phase products

The composition of the reactor effluent as determined by GC–FID after 60 s of co-reaction of benzene and methanol at 350 °C for the three catalysts is given in Table 1. Methanol and dimethyl ether, which are rapidly equilibrated, and benzene, which is a very minor product in the MTH reaction, are considered to be unconverted reactants in this experiment. Thus, the combined conversion was in the range 92 to 96% for the three catalysts. At such high conversions, it is difficult to establish small activity differences. In order to compare the activities at a lower conversion level, a similar set of data was also obtained at 300 °C, giving the following conversions: H-beta: 42%; H-mordenite: 42%; H-MCM-22: 31%. Thus, H-MCM-22 has a somewhat lower activity compared to the other two samples, but it is reasonable to conclude that there are no large activity differences among the materials. We note that the lower concentration of acid sites in the H-mordenite catalyst (Si/Al = 22) is not reflected in a lower conversion level than observed for H-beta (Si/Al = 12). The products formed are typical for the MTH reaction over the three Al-rich catalysts [28,38,40]. For H-beta, butanes and hexaMB are the major products, as reported by Bjørgen and Kolboe [28]. Similar observations are made for H-mordenite, except that pentaMB is

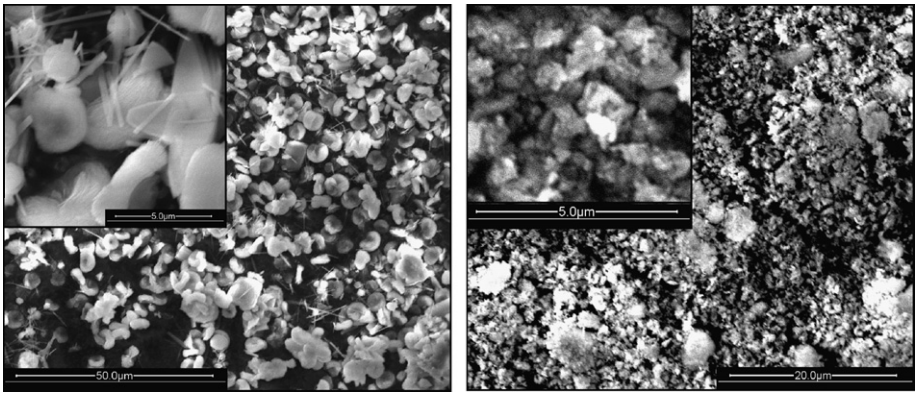

Fig. 2. SEM micrographs of H-MCM-22 (left panel) and H-mordenite (right panel).

Table 1
Effluent composition (in C%) after 60 s of benzene/methanol reaction over the different zeolite samples at 350 °C.

Compound	H-beta	H-mordenite	H-MCM-22
MeOH/DME	2.4	0.3	3.0
Methane	0.3	0.5	1.0
Ethene	13.3	6.6	13.4
Propane	6.2	3.7	17.9
Propene	6.3	13.0	3.3
Butanes	34.7	23.9	38.1
Butenes	1.2	3.5	1.0
C_5	10.0	6.4	15.2
C_6	3.3	2.2	5.7
Benzene	5.5	5.0	1.4
PentaMB	–	22.4	–
HexaMB	16.9	12.7	–
C_3-HTI *	*0.50*	*0.22*	*0.84*
C_4-HTI	*0.97*	*0.85*	*0.97*

* C_i hydrogen transfer index; HTI = C_i alkanes/(C_i alkanes + C_i alkenes); i = carbon number.

formed in larger amounts than hexaMB. Aramendia et al. [40] studied the conversion of methanol over H-mordenite (Si/Al = 45) and also found a higher selectivity toward pentaMB than toward hexaMB. As mentioned by Armendia et al. [40], this might signify that the diffusion of hexaMB through the pores of H-mordenite is slower than in the slightly more spacious H-beta. However, crystal size effects, i.e. longer diffusion pathways for H-mordenite, might also play a role. For H-MCM-22, however, no noticeable amounts of aromatics are detected in the effluent; the main products are saturated aliphatics in the C_3–C_5 range. The predominant production of alkanes signifies that large amounts of hydrogen-poor material are retained within the cages of H-MCM-22 in order to match the H:C ratio of ~1.5 in the methanol/benzene feedstock (as is indeed confirmed below). The lower aromatics such as xylenes, which are typical products for 10-ring zeolites, are not seen among the products for this H-MCM-22 sample. However, the 10-ring apertures of H-MCM-22 are notably smaller than those seen for e.g. H-ZSM-5 (see Section 3.1), so if the product selectivity is governed strictly by the 10 rings, aromatics might not be able to diffuse out of the crystals and into the gas phase. Indeed, the analysis of the retained material at 350 °C (see below) does show that there is significantly more triMB retained in H-MCM-22 than in the strict 12-ring systems. Ravishankar et al. [38] observed significant amounts of hexaMB in the effluent during the conversion of methanol over H-MCM-22 (Si/Al = 14), but it seems plausible that this is related to non-shape-selective catalytic reactions occurring in the pockets on the external surface of the catalyst [37,41].

Significant differences in hydrogen transfer activity are seen among the three catalysts. The hydrogen transfer activity may be conveniently assessed by the hydrogen transfer index (HTI), which has been defined by Tsang et al. [42] as the ratio between the yield of alkanes and the yield of alkanes + alkenes for a given carbon chain length. It should be kept in mind that these experiments have been carried out with the somewhat unusual H:C ratio of ~1.5 in the feedstock. This means that alkane formation in this case is associated with formation of compounds even poorer in hydrogen than the monoaromatic methylbenzenes (the H:C ratio in hexaMB is 1.5), such as naphthalenic species. For H-MCM-22, the C_3-HTI is noticeably larger than what is found for H-beta and in particular H-mordenite. This is most likely linked to the particular shape-selective properties of this material induced by the more narrow 10 rings in H-MCM-22, as mentioned earlier: the product molecules actually formed are to a larger extent withheld in the cages of H-MCM-22 and experience a longer effective contact time. This will favor the hydrogen transfer reactions, which may be considered to be secondary to the alkene formation. For H-beta and H-MCM-22, the C_4-HTI is close to unity, implying that virtually all butenes become saturated. It is reasonable that hydrogen transfer reactions are quicker for the butenes than the propene; the proton affinity of the butenes are higher than for propene, and the hydrogen transfers will take place via carbenium ion-like intermediates. Overall, H-mordenite displays the lowest hydrogen transfer activity, in line with the lower acid site density [43].

3.4. Analyses of the retained hydrocarbons by dissolution in HF and extraction

The hydrocarbons retained within the pores of the three catalysts were analyzed by the dissolution/extraction technique after 90 s of ^{12}C benzene/^{13}C methanol co-reaction at several reaction temperatures. The GC–MS total ion chromatograms thus obtained are displayed for the three catalysts in Figs. 3–5. Similar, but not identical, results have been presented for H-beta previously [10]. Starting with H-beta, at low reaction temperatures, methylation of benzene is the all-dominant reaction. The benzene ring is methylated up to seven times, eventually leading to the non-aromatic and highly reactive heptaMB$^+$. This species is detected after HF dissolution/extraction as the conjugate base HMMC and is eluted before hexaMB. At 225 °C, hexaMB is in excess when compared to heptaMB$^+$/HMMC, and this will be elaborated below. Also, small amounts of pentaMB and traces of the lower methylbenzenes are seen. Diphenylmethane, which most likely is formed by the reaction between toluene and benzene [10], is also seen at the lowest temperatures. Its formation may be considered to be an effect of the high concentration of benzene in the co-reaction and is not re-

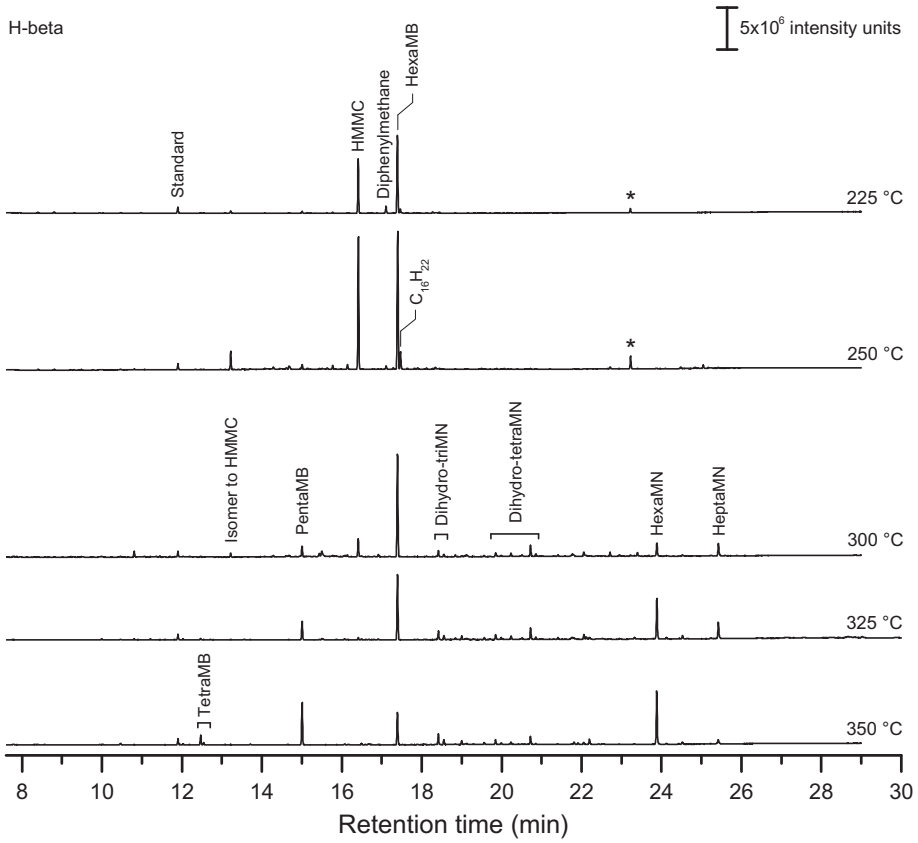

Fig. 3. GC–MS total ion chromatograms of material retained in H-beta after 90 s of co-reaction of methanol and benzene.

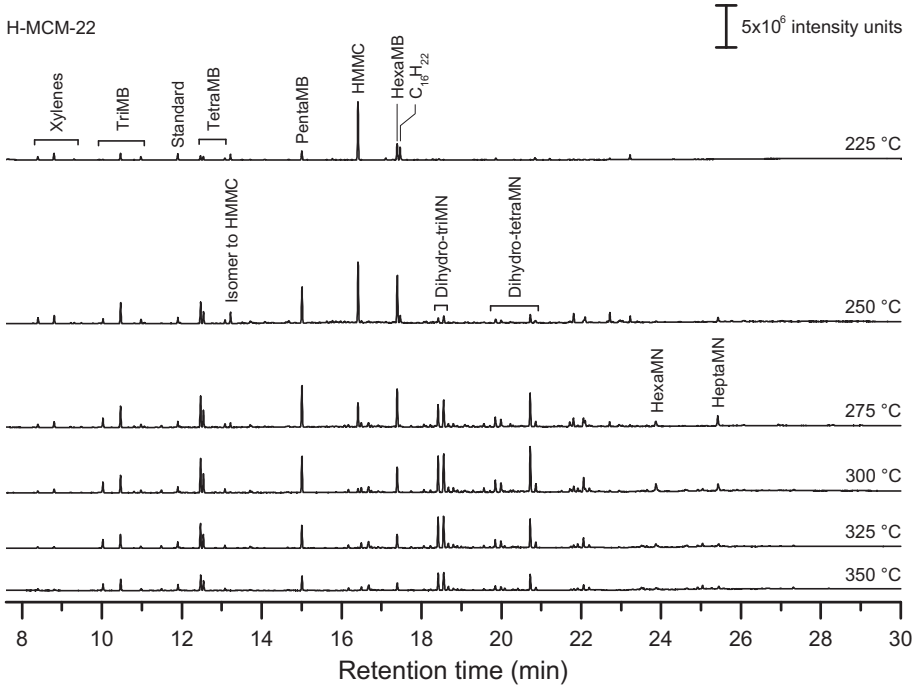

Fig. 4. GC–MS total ion chromatograms of material retained in H-MCM-22 after 90 s of co-reaction of methanol and benzene.

lated to the actual MTH chemistry. The peak denoted by an asterisk is not an actual product formed in the benzene/methanol co-reaction but is the outcome of a reaction between heptaMB$^+$/HMMC and the CCl_4 solvent [10]. As the temperature is increased to 250 °C, both hexaMB and heptaMB$^+$/HMMC increase, but this is much more pronounced for heptaMB$^+$/HMMC. In addition, a structural isomer to heptaMB$^+$/HMMC appears at shorter retention times. Quantum chemical calculations have indicated that, in the

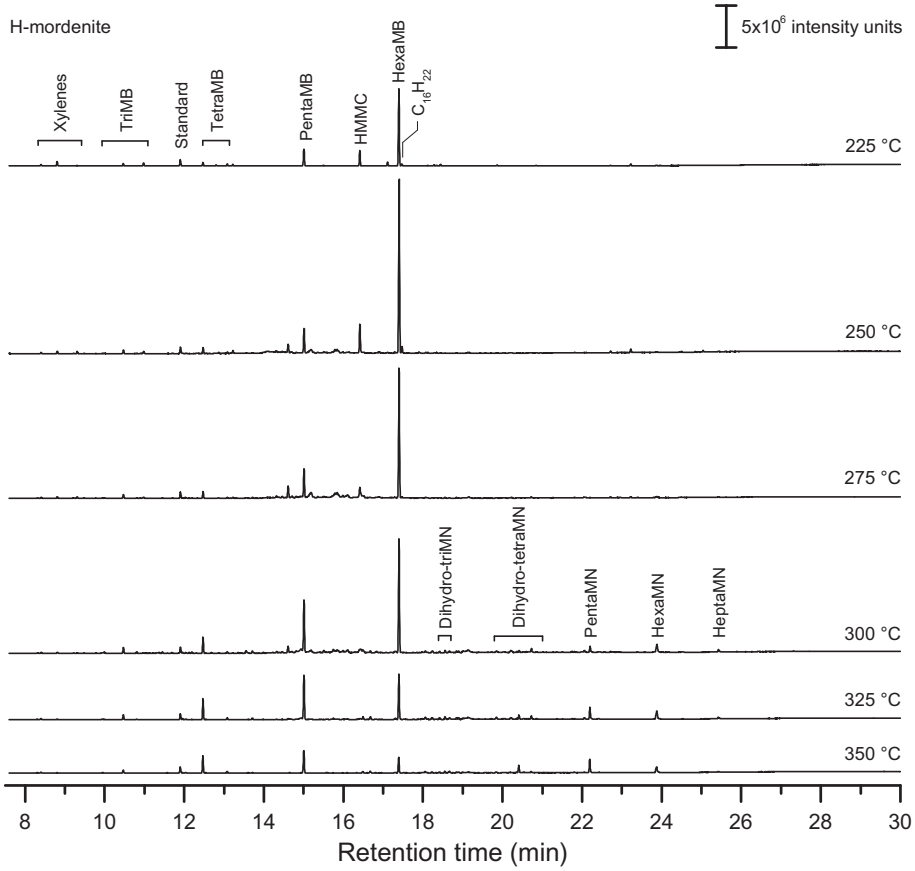

Fig. 5. GC–MS total ion chromatograms of material retained in H-mordenite after 90 s of co-reaction of methanol and benzene.

absence of steric hindrance, there is a gradual decrease in the activation energy for the methylation reaction with the number of methyl groups [44], i.e. given sufficient space, the methylation of hexaMB to form heptaMB$^+$/HMMC is quicker than the methylation of pentaMB to form hexaMB. Consequently, the fact that there is less heptaMB$^+$/HMMC than hexaMB at 225 °C indicates that the formation of heptaMB$^+$/HMMC might be restricted. The most plausible explanation for this is that steric limitations are imposed on the final methylation step by the zeolite lattice. As the temperature is further increased to 300 °C, both hexaMB and heptaMB$^+$/HMMC decrease in abundance, but much more markedly for heptaMB$^+$/HMMC. This is related to the particular importance of heptaMB$^+$/HMMC as an intermediate in alkene formation [11]. In this temperature range, alkene formation becomes pronounced [10], and the system is no longer completely described by simple methylation steps (see Section 3.5). According to the paring reaction scheme, hexaMB and heptaMB$^+$/HMMC will eliminate light alkenes under concomitant formation of lower methylbenzenes. Consequently, the concentrations of lower methylbenzenes tend to increase when the concentrations of hexaMB and heptaMB$^+$/HMMC decrease. This development seen for the methylbenzenes continues at 325 and 350 °C. HeptaMB$^+$/HMMC is barely detectable at 325 and vanishes completely at 350 °C. In parallel, the tetraMBs increase substantially (by a factor of ~6 for the most prominent isomer) and pentaMB is more than doubled.

At 300 °C, various naphthalene derivatives ranging from dihydrotriMN to heptaMN also appear in the extract. See Scheme 2 for a depiction of the naphthalenic species. The exact substitution pattern on the bicyclic carbon skeleton is uncertain. Notably, lower naphthalene derivatives are not detected. This occurs in the same temperature range as the lower methylbenzenes increase and significant alkene formation takes place. It has been shown that methylnaphthalenes have some reactivity in alkene-forming reactions, analogous to the methylbenzenes, but these compounds have also been identified as coke precursors that eventually lead to catalyst deactivation [9,10,45]. It appears that ring condensation reactions become significant at about the same reaction temperature as the lower methylbenzenes increase as a result of alkene formation. This indicates that the formation of bicyclic compounds, which eventually leads to catalyst deactivation by coking, is inherently linked to the desired alkene formation. The formation of bicyclic compounds will be further elaborated in Section 3.5.

The lower methylnaphthalene derivatives, dihydrotriMN and dihydrotetraMN, are present in approximately unaltered amounts at 300, 325, and 350 °C, whereas a significant evolution with temperature is seen for hexaMN and heptaMN. HexaMN increases, whereas a maximum is reached for heptaMN at 325 °C. This behavior of passing through a concentration maximum is analogous to what was observed for hexaMB and heptaMB$^+$/HMMC and could suggest that heptaMN might also serve as an intermediate in alkene formation, as suggested previously [45]. The maximum in the concentration of heptaMN occurs at a reaction temperature that is about 75 °C higher than the temperature where heptaMB$^+$/HMMC is at its maximum (250 °C), and this might be indicative of the difference in their reactivity as intermediates for alkene formation. A similar conclusion was reached by Song et al. [45], although in their work a smaller reactivity difference between methylbenzenes and methylnaphthalenes than what is implied by a temperature difference of 75 °C was reported.

Fig. 4 displays the GC–MS analyses of the material retained the cavities of H-MCM-22 after 90 s of benzene/methanol co-reaction in the 225–350 °C reaction temperature range. Despite the signifi-

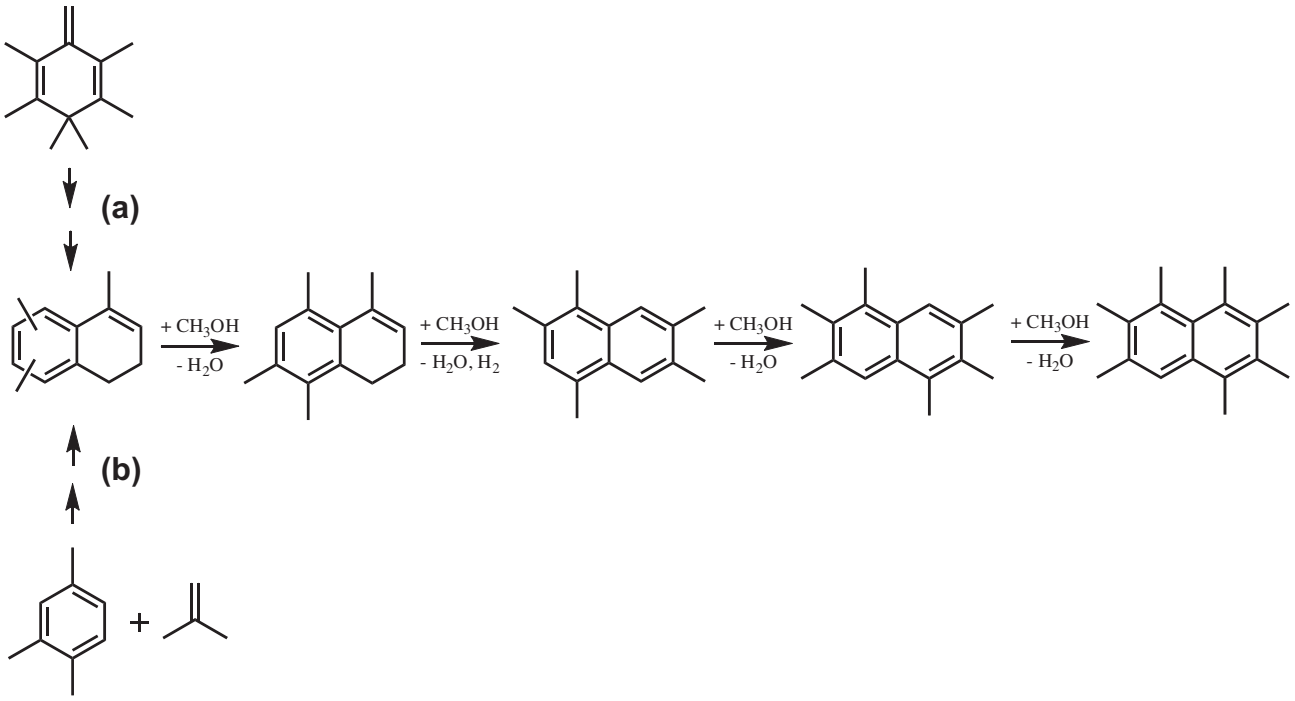

Scheme 2. Pathways (a) and (b) are suggested possibilities for the formation of dihydrotriMN, which may undergo a series of methylation steps to form heptaMN. The final hydride transfer occurs in the transition from dihydrotetraMN to pentaMN.

cant differences in catalyst topologies, the hydrocarbons built up in H-MCM-22 and H-beta during the reaction are very similar. Significant differences in concentrations are observed and will be discussed below, but it should be emphasized that all of the prominent compounds detected in H-beta are also found in H-MCM-22 and vice versa. Importantly, as the MTH reaction is known to proceed indirectly via adsorbed intermediates such as hexaMB and heptaMB$^+$/HMMC, this observation strongly implies extensive mechanistic similarities between the two catalysts. Perusal of Fig. 4 also reveals quite similar temperature effects on the retained material in the two catalysts. At 225 °C, hexaMB and heptaMB$^+$/HMMC are dominant, as was the case for H-Beta. In addition, significant amounts of the other methylbenzenes, from the xylenes and up are also seen. These compounds were not nearly as prominent in the pores of H-beta, and additionally previous studies [10] carried out at the same conditions have shown that there are no xylenes, triMBs, tetraMBs, or pentaMB in the effluent from H-beta below 250 °C. Thus, these compounds are most probably located in the second, isolated pore system of H-MCM-22 comprised exclusively of 10 rings. Also, more heptaMB$^+$/HMMC relative to hexaMB is seen in H-MCM-22 compared to H-beta. This signifies that the final methylation step is quicker in H-MCM-22. However, the effect of reaction temperature on the concentration of heptaMB$^+$/HMMC in the pores is similar for the two catalysts; heptaMB$^+$/HMMC declines more rapidly with increasing temperature than the other compounds when the reaction temperatures pass above 250 °C, underlining the special importance of this compound as a reaction intermediate in the MTH reaction also for H-MCM-22. Fig. 4 shows the first observation of heptaMB$^+$/HMMC in a material other than H-beta. Previous detailed investigations of the hydrocarbon pool mechanism have been carried out only for a limited number of catalyst topologies (MFI, CHA, BEA), and the profound similarities between H-beta and H-MCM-22 shown here constitute a significant step toward a unified understanding of the MTH reaction over acidic zeolites.

From reaction temperatures of 250 °C and above, the retained material in H-MCM-22 shows a development with increasing reac-

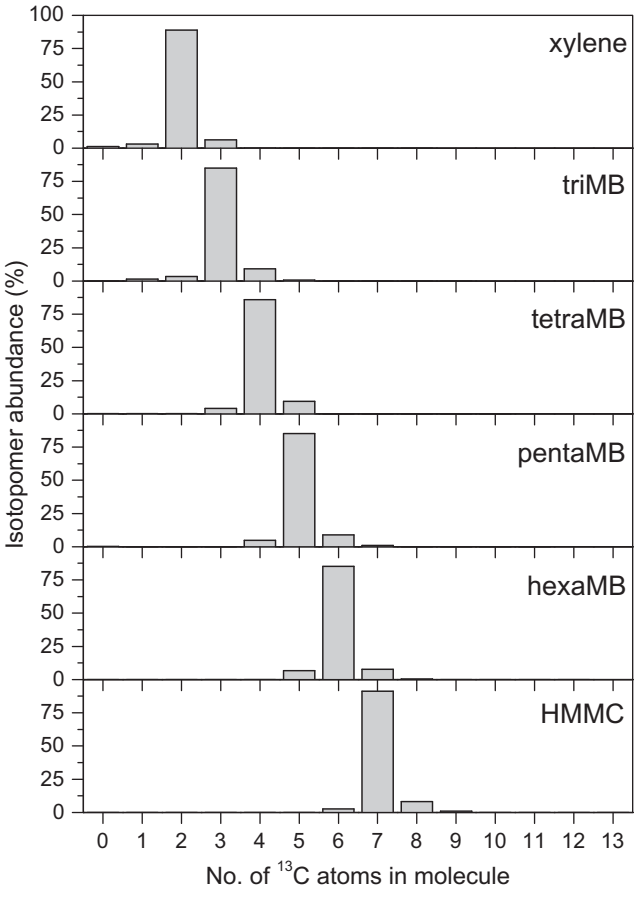

Fig. 6. Isotopomer distribution for the methylbenzenes retained in H-mordenite after 90 s of co-reaction of benzene and methanol at 225 °C.

tion temperature similar to that seen at 300 °C in H-beta. Naphthalene derivatives are formed and the lower methylbenzenes increase at the expense of hexaMB and heptaMB$^+$/HMMC. This is linked to alkene formation, as discussed above. Also in this material, dihydrotriMNs are the lowest naphthalene derivatives detected, implying that the same reaction steps involved in the second ring condensations are operative in H-MCM-22. HeptaMN is the heaviest naphthalene derivative detected in significant amounts in both materials, suggesting that the formation of octaMN is highly unfavorable. A maximum in the concentration of heptaMN is seen at 275 °C, which is significantly lower than in H-beta.

Despite the relatively large differences in concentrations of the various compounds retained in H-mordenite (Fig. 5) when compared to the other two catalysts, it is indeed the same compounds that are detected, and the overall results serve to consolidate the conclusions already reached. Again heptaMB$^+$/HMMC is detected, meaning that this compound is commonly formed during the MTH reaction over large cavity zeolites. The concentration of heptaMB$^+$/HMMC is observed to pass through a concentration maximum at 250 °C, thereafter diminishing rapidly as the reaction temperature is further increased. However, it appears that the formation of heptaMB$^+$/HMMC in H-mordenite is more restricted than in H-beta, because hexaMB is in excess by no less than a factor of ~6 at any reaction temperature, whereas the two compounds are present in comparable concentration in the other catalysts. Thus, the oval, non-intersecting linear 12-ring pores of H-mordenite appear to be slightly less spacious than the pores of H-beta and in particular the cavities of H-MCM-22. This is in line with the topologies as described above. As the concentration of hexaMB and heptaMB$^+$/HMMC is reduced at ~275 °C, both the lower methylbenzenes and the naphthalene derivatives tend to increase, even though the naphthalene derivatives are much less copious in H-mordenite compared to the two other zeolites. Even so, hexa- and heptaMN are the heaviest compounds formed also in H-mordenite, and they pass through a concentration maximum at 300/325 °C. Finally, we note that the full dehydrogenation of the bicyclic naphthalene carbon skeleton occurs in the transition dihydrotetraMN/pentaMN also for H-mordenite.

3.5. Isotopic composition of the retained material

The co-reaction of methanol and benzene was carried out using ^{13}C-labeled methanol and ^{12}C benzene, and the isotopic composition of the retained material was determined. This allows us to distinguish between carbon atoms originating from each of the two reactants. An extensive dataset was thus obtained, and we will emphasize the main trends observed. As is clear from Figs. 3–5, not all compounds are present in each zeolite at every reaction temperature. Therefore, a representative selection of the total data will be presented.

First, we will examine the isotopic composition of the methylbenzenes, from xylene to HMMC at 225 °C in H-mordenite, presented in Fig. 6. Clearly, the isotopomers originating from repeated methylation of benzene dominates throughout this series: the number of ^{13}C atoms matches the number of methyl groups for the dominant isotopomer (85–90%). This confirms that sequential methylation of benzene is the prevailing reaction occurring at low reaction temperatures. Alkene formation does not occur at 225 °C, and it may confidently be inferred that each of the individual methylation steps are quicker than the reaction steps leading to alkenes.

At higher reaction temperatures, this methylation pattern is obscured, as the alkene-forming reactions lead to a broadening of the

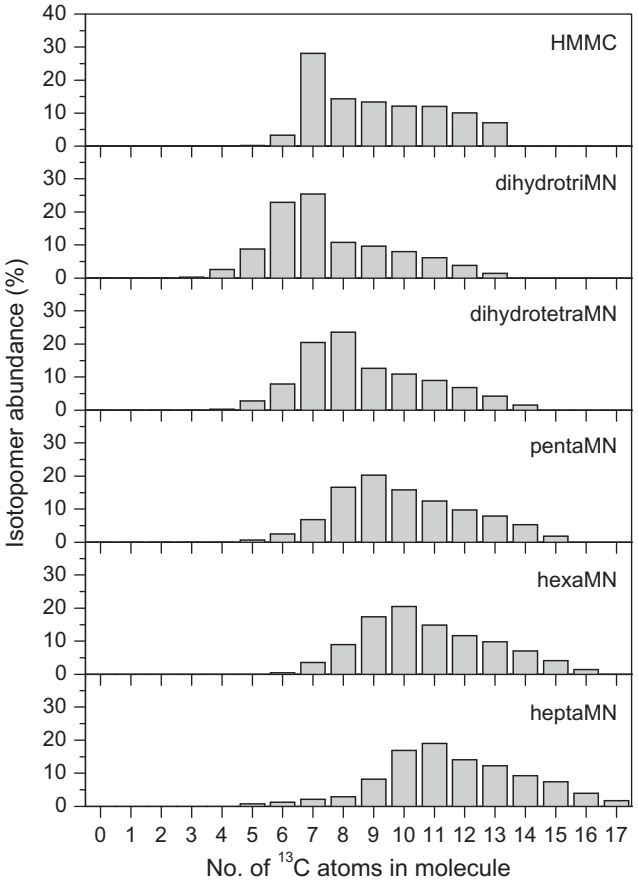

Fig. 7. Isotopomer distribution for HMMC and the methylnaphthalenes retained in H-MCM-22 after 90 s of co-reaction of benzene and methanol at 300 °C.

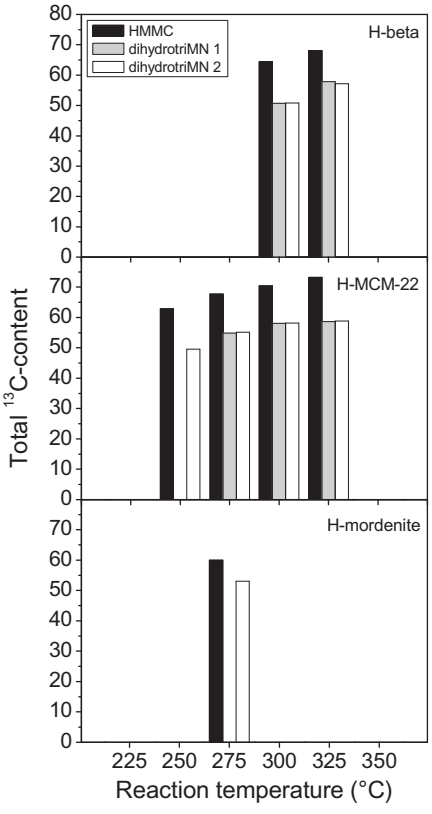

Fig. 8. Total content of ^{13}C in HMMC and two dihydrotriMN isomers retained in the three zeolites after 90 s of co-reaction of benzene and methanol at various temperatures.

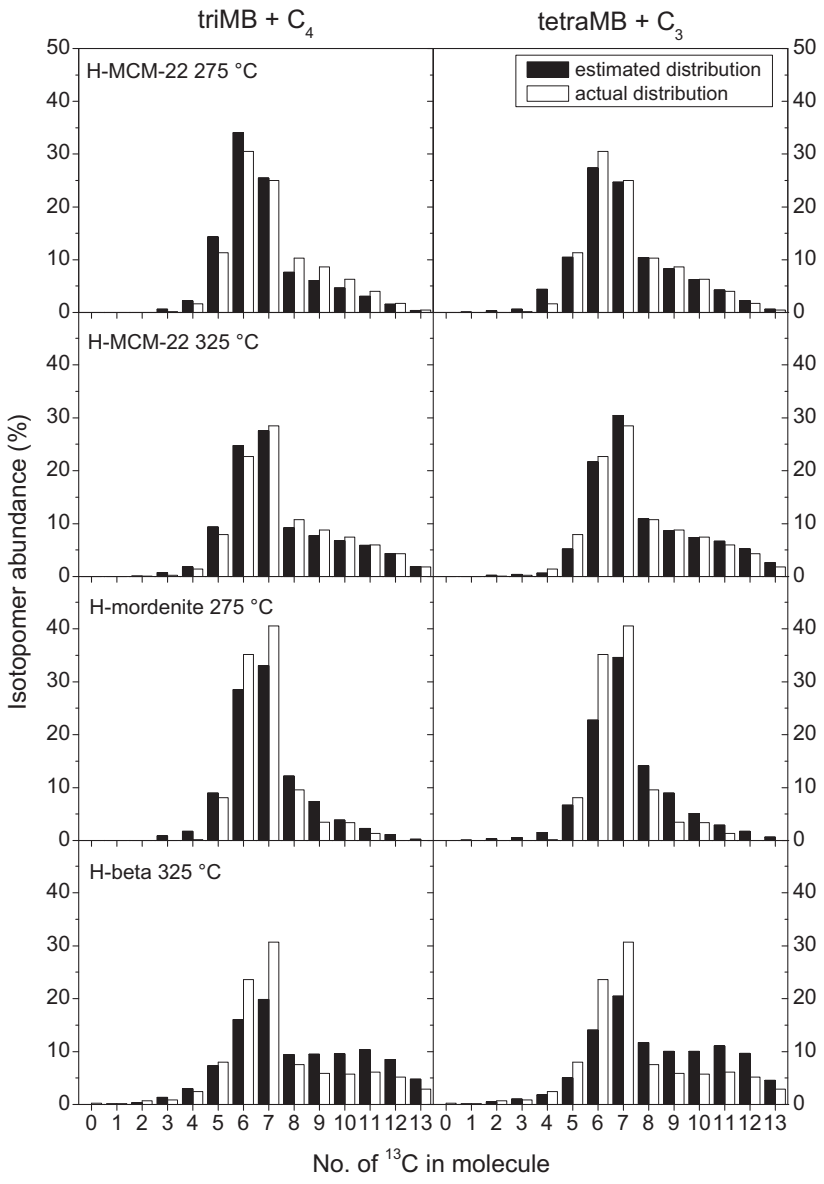

Fig. 9. Actual (white bars) and predicted isotopic distributions (black bars) of dihydrotriMN. The predicted distributions are obtained by assuming either the coupling of triMB and a representative C_4 aliphatics species (left column) or coupling of tetraMB and C_3 (right column).

isotopomer distributions. This has been described and discussed extensively previously [10], and will not be repeated here. The effect is shown for HMMC at 300 °C in H-MCM-22 in the top panel of Fig. 7. However, another feature is clearly borne out by Fig. 7. Starting with dihydrotriMN (the smallest observable bicyclic compound in all three catalysts), another methylation series is evident: the distributions are shifted in steps of one as the number of methyl groups on the naphthalene skeleton increases. This means that dihydrotriMN is the precursor for the largest species detected in these experiments via sequential methylation, as shown in Scheme 2. What is then the origin of dihydrotriMN? The fact that no dihydro*di*methylnaphthalene or *di*methylnaphthalene is observed indicates that dihydrotriMN is indeed the primordial bicyclic compound, for several catalysts. It is noteworthy that the number of C-atoms in dihydrotriMN is the same as for HMMC and that dihydrotriMN is the smallest naphthalene derivative detected. A rearrangement of HMMC into dihydrotriMN has previously been suggested (pathway a in Scheme 2) [9], but as seen in Fig. 7, the isotopic composition of HMMC is clearly different from that of dihydrotriMN. For dihydrotriMN, the isotopomer with 6 ^{13}C atoms is in excess compared to HMMC. This is a general feature for all three catalysts at all temperatures: Fig. 8 shows the total ^{13}C content in HMMC and two dihydrotriMN isomers for the conditions at which all species are present at amounts sufficient for reliable analysis. Very clearly, the discrepancy is general. This suggests that a simple, direct formation of dihydrotriMN from HMMC does not properly account for the observations made.

The issue then becomes to find a mechanistic rationale for the apparent excess of ^{12}C in dihydrotriMN. Sassi et al. [17] have proposed that coupling of alkyl groups on the benzene ring might lead to bicyclic species. Substituents on the ring larger than methyl groups are hypothesized to be formed during both the paring and side-chain reaction mechanisms, but neither route can explain why there generally is less ^{13}C in dihydrotriMN than in HMMC. However, if C_{2+} alkyl chains are indeed required to form bicyclic compounds, these chains might alternatively be formed by alkylation of methylbenzenes by alkene products. The alkenes in the gas phase are known to contain less than 100% ^{13}C, as some of

the carbon atoms originate from the benzene rings [9]. To investigate this possibility, we determined the isotopic distribution of propane/propene and the butanes/butenes in the effluent. It is then possible to estimate the isotopic composition of a C_{13} species formed by the combination of triMB and C_4 or by combination of tetraMB and C_3 (pathway b in Scheme 2) for comparison with the observed isotopic distribution in dihydrotriMN. (The isotopic distribution of the alkenes could not always be analyzed with sufficient accuracy, and the alkanes, which are abundant in the effluent, can be assumed to be representative for the more reactive alkenes.) The estimated isotopic distributions for dihydrotriMN thus obtained are compared to the actual distributions in Fig. 9. Clearly, the agreement between the predicted and actual isotopic distributions is remarkable for H-MCM-22 at two temperatures. This lends support to the idea that interaction between a methylbenzene and an aliphatic species is required for the formation of bicyclic compounds (pathway b in Scheme 2). This issue is of high relevance; as such species are much likely to be coke precursors leading to catalyst deactivation. However, the data are less convincing for H-beta and H-mordenite, but this assumption does provide a qualitative explanation for the lower ^{13}C content in dihydrotriMN when compared to HMMC. It does not, on the other hand, explain why naphthalene derivatives with fewer than 13 C-atoms are not found in the effluent. It is not straightforward to realize why the coupling of e.g. xylenes and a C_4 fragment, leading to a bicyclic species with only 12 C-atoms (which are not detected), should be prohibited.

3.6. Quantum chemical calculations

Two issues were attempted that was addressed using computational methods.

First, heptaMN is the largest naphthalene derivative found in substantial amounts for all three zeolites, and octaMN is insignificant. Is this caused by an inherent instability of the most substituted naphthalene or by steric restrictions imposed by the zeolite lattice limiting the growth of this species? Table 2 lists the enthalpies and Gibbs free energies for this whole series of methylation steps, from naphthalene to octaMN. The data in Table 2 are based on the most stable isomer for each carbon number. The data for the other isomers are given in Supplementary material. The enthalpy and free energy of the methylation reactions are similar for all congeners up to the formation of pentaMN. The formation of hexaMN is clearly less favorable, the formation of heptaMN and octaMN even more so. However, all reactions are exothermic and exergonic; so that no step of the methylation series becomes thermodynamically prohibited. Even so, the formation of hepta- and octaMN is much less exothermic/exergonic than the formation of the lower congeners. This is certainly caused by the internal steric stress in the highly substituted naphthalenes; in octaMN, the arrangement of the 18 carbon atoms deviates strongly from the planar situation that one might expect. The calculations thus show that there is a thermodynamic factor to the apparently limited formation of hepta- and octaMN, but the limited space within the zeolite voids must play the major role.

Table 2
Enthalpies and Gibbs free energies (at 298.15 K) of methylation for various naphthalene derivatives calculated using two different methods.

Methylation reaction	G3MP2B3 (kJ/mol)	
	$\Delta_r H°$	$\Delta_r G°$
Naphthalene → 2-MN	−75	−75
2-MN → 2,8-diMN	−74	−69
2,8-diMN → 2,3,7-triMN	−74	−69
2,3,7-triMN → 2,3,6,7-tetraMN	−74	−63
2,3,6,7-tetraMN → 1,2,4,6,7-pentaMN	−66	−65
1,2,4,6,7-pentaMN → 1,2,3,5,6,7-hexaMN	−54	−49
1,2,3,5,6,7-hexaMN → 1,2,3,4,5,6,7-heptaMN	−32	−25
1,2,3,4,5,6,7-heptaMN → 1,2,3,4,5,6,7,8-octaMN	−34	−23
Dihydrotetramn → dihydropentaMN	−60	−58

Second, we observe dihydrotri- and dihydrotetraMN in the extracts, but not dihydropentaMN. This might be caused by unfavorable thermodynamics for the addition of the fifth methyl group or it might mean that dihydropentaMN, when formed, is immediately dehydrogenated into pentaMN upon formation. As indicated by the data in Table 2, which is based on a reasonable selection of isomers, there is no thermodynamic limitation to the methylation of dihydrotetraMN into dihydropentaMN. This indicates that for dihydropentaMN hydride, transfers leading to dehydrogenation are much more rapid than methylation. This, in turn, is most likely related to proton affinities and longevities of the various species involved in the hydride transfers leading to dehydrogenation of dihydropentaMN.

4. Summary and conclusions

Striking similarities have been observed for composition and the reaction pattern of the retained material in the three catalysts, despite the apparent complexity. We have now made a significant step toward a generalization of the validity of observations and conclusions previously obtained for H-beta and H-SAPO-34, at least for large cavity catalysts, i.e. materials comprising pores defined by 12-membered rings:

(1) It is the same hydrocarbon compounds that are built up and retained in the three different zeolite topologies.
(2) Their reactivity, inferred from the changes in concentration as a function of temperature and isotopic composition, is also very similar. The higher methylbenzenes, hexaMB in H-mordenite, and heptaMB$^+$/HMMC in H-beta and H-MCM-22 are easily formed at the lowest temperatures and gradually vanish as significant alkene formation occurs when the temperature is increased. Simultaneously, the lower methylbenzenes appear in the extracts. This is consistent with the aromatics-based hydrocarbon pool mechanism and is the manifestation of the role of the highest methylbenzenes as important reaction intermediates for all three catalysts.
(3) The fact that the very highest methylated benzenes are readily formed as the dominant species via simple methylations at reactions temperatures where alkene formation is insignificant, strongly suggests that it is the decomposition (via the paring route) or further reaction (via side-chain methylation) of these species that is the rate-determining step in MTH reaction for these three large cavity zeolites.
(4) DihydrotriMN is found to be the smallest bicyclic compound formed in all three catalysts. However, the isotopic composition is not in exact agreement with a previously proposed rearrangement of heptaMB$^+$/HMMC leading to dihydrotriMN. An alternative mechanism, involving the coupling of a methylbenzene and an aliphatic species could explain the observed isotopic distributions. We emphasize, however, that these suggestions are hypotheses only and that further work is required to pinpoint how bicyclic compounds, which are pivotal in the processes leading to catalyst deactivation, are formed.
(5) DihydrotriMN is the precursor for the formation of the heaviest species detected, heptaMN, through a series of methylation reactions. DihydropentaMN is not seen in the retained material, despite there being no thermodynamic

limitation to the methylation of dihydrotetraMN. Thus, for dihydropentaMN, dehydrogenation to form the fully aromatic carbon skeleton is much faster than further methylation steps.

(6) The concentrations of hexaMN and heptaMN in the retained material go through maxima in much the same way as seen for hexaMB and heptaMB$^+$/HMMC, although at about 50 °C higher temperatures. This might indicate that these species may function as hydrocarbon pool species, albeit much less efficient than the methylbenzenes.

(7) Taken together, the results presented here serve to consolidate the conclusions reached previously for the H-beta zeolite. It appears that the formation of heptaMB$^+$/HMMC is a quite general feature for large cavity zeolites and that the highest methylbenzenes function as reaction intermediates in the MTH reaction.

Acknowledgments

This publication is part of the inGAP Center of Research Based Innovation, which receives financial support from the Norwegian Research Council under Contract No. 174893. Thanks are also due to the Research Council of Norway for Grant of computer time through the NOTUR Project (Account NN4683K).

Appendix A. Supplementary data

Supplementary data associated with topologies, energies of the methyl naphthalenes and BET-isotherms can be found, in the online version, at doi:10.1016/j.jcat.2010.08.001.

References

[1] J.F. Haw, W. Song, D.M. Marcus, J.B. Nicholas, Acc. Chem. Res. 36 (2003) 317.
[2] U. Olsbye, M. Bjørgen, S. Svelle, K.P. Lillerud, S. Kolboe, Catal. Today 106 (2005) 108.
[3] I.M. Dahl, S. Kolboe, Catal. Lett. 20 (1993) 329.
[4] I.M. Dahl, S. Kolboe, J. Catal. 149 (1994) 458.
[5] B. Arstad, S. Kolboe, Catal. Lett. 71 (2001) 209.
[6] B. Arstad, S. Kolboe, J. Am. Chem. Soc. 123 (2001) 8137.
[7] B.P.C. Hereijgers, F. Bleken, M.H. Nilsen, S. Svelle, K.P. Lillerud, M. Bjørgen, B.M. Weckhuysen, U. Olsbye, J. Catal. 264 (2009) 77.
[8] F. Bleken, M. Bjørgen, L. Palumbo, S. Bordiga, S. Svelle, K.P. Lillerud, U. Olsbye, Top. Catal. 52 (2009) 218.
[9] M. Bjørgen, U. Olsbye, S. Kolboe, J. Catal. 215 (2003) 30.
[10] M. Bjørgen, U. Olsbye, D. Petersen, S. Kolboe, J. Catal. 221 (2004) 1.
[11] M. Bjørgen, U. Olsbye, S. Svelle, S. Kolboe, Catal. Lett. 93 (2004) 37.
[12] W.vonE. Doering, M. Saunders, H.G. Boyton, H.W. Earhart, E.F. Wadley, W.R. Edwards, G. Laber, Tetrahedron 4 (1958) 178.
[13] S. Svelle, M. Bjørgen, S. Kolboe, D. Kuck, M. Letzel, U. Olsbye, O. Sekiguchi, E. Uggerud, Catal. Lett. 109 (2006) 25.
[14] S. Kolboe, S. Svelle, B. Arstad, J. Phys. Chem. A 113 (2009) 917.
[15] T. Mole, J.A. Whiteside, D.J. Seddon, J. Catal. 82 (1983) 261.
[16] T. Mole, G. Bett, D.J. Seddon, J. Catal. 84 (1983) 435.
[17] A. Sassi, M.A. Wildman, H.J. Ahn, P. Prasad, J.B. Nicholas, J.F. Haw, J. Phys. Chem. B 106 (2002) 2294.
[18] W. Song, J.F. Haw, J.B. Nicholas, C.S. Heneghan, J. Am. Chem. Soc. 122 (2000) 10726.
[19] M. Bjørgen, S. Svelle, F. Joensen, J. Nerlov, S. Kolboe, F. Bonino, L. Palumbo, S. Bordiga, U. Olsbye, J. Catal. 249 (2007) 193.
[20] S. Svelle, F. Joensen, J. Nerlov, U. Olsbye, K.P. Lillerud, S. Kolboe, M. Bjørgen, J. Am. Chem. Soc. 128 (2006) 14770.
[21] M. Bjørgen, F. Joensen, K.P. Lillerud, U. Olsbye, S. Svelle, Catal. Today 142 (2009) 90.
[22] M. Bjørgen, K.P. Lillerud, U. Olsbye, S. Svelle, Stud. Surf. Sci. Catal. 167 (2007) 463.
[23] S. Svelle, U. Olsbye, F. Joensen, M. Bjørgen, J. Phys. Chem. C 111 (2007) 17981.
[24] R.M. Dessau, J. Catal. 99 (1986) 111.
[25] P.O. Rønning, Ph.D. thesis, University of Oslo, 1998.
[26] I. Güray, J. Warzywoda, N. Bac, A. Sacco, Micropor. Mesopor. Mater. 31 (1999) 241.
[27] M. Bjørgen, K.P. Lillerud, U. Olsbye, S. Bordiga, A. Zecchina, J. Phys. Chem. B 108 (2004) 7862.
[28] M. Bjørgen, S. Kolboe, Appl. Catal. A 225 (2002) 285.
[29] S. Svelle, U. Olsbye, K.P. Lillerud, S. Kolboe, M. Bjørgen, J. Am. Chem. Soc. 128 (2006) 5618.
[30] P. Magnoux, P. Roger, C. Canaff, V. Fouche, N.S. Gnep, M. Guisnet, Stud. Surf. Sci. Catal. 34 (1987) 317.
[31] M.J. Frisch, G.W. Trucks, H.B. Schlegel, G.E. Scuseria, M.A. Robb, J.R. Cheeseman, J.A. Montgomery Jr., T. Vreven, K.N. Kudin, J.C. Burant, J.M. Millam, S.S. Iyengar, J. Tomasi, V. Barone, B. Mennucci, M. Cossi, G. Scalmani, N. Rega, G.A. Petersson, H. Nakatsuji, M. Hada, M. Ehara, K. Toyota, R. Fukuda, J. Hasegawa, M. Ishida, T. Nakajima, Y. Honda, O. Kitao, H. Nakai, M. Klene, X. Li, J.E. Knox, H.P. Hratchian, J.B. Cross, V. Bakken, C. Adamo, J. Jaramillo, R. Gomperts, R.E. Stratmann, O. Yazyev, A.J. Austin, R. Cammi, C. Pomelli, J.W. Ochterski, P.Y. Ayala, K. Morokuma, G.A. Voth, P. Salvador, J.J. Dannenberg, V.G. Zakrzewski, S. Dapprich, A.D. Daniels, M.C. Strain, O. Farkas, D.K. Malick, A.D. Rabuck, K. Raghavachari, J.B. Foresman, J.V. Ortiz, Q. Cui, A.G. Baboul, S. Clifford, J. Cioslowski, B.B. Stefanov, G. Liu, A. Liashenko, P. Piskorz, I. Komaromi, R.L. Martin, D.J. Fox, T. Keith, M.A. Al-Laham, C.Y. Peng, A. Nanayakkara, M. Challacombe, P.M.W. Gill, B. Johnson, W. Chen, M.W. Wong, C. Gonzalez, J.A. Pople, Gaussian 03, Revision D.02, Gaussian, Inc., Wallingford CT, 2004.
[32] A.G. Baboul, L.A. Curtiss, P.C. Redfern, K. Raghavachari, J. Chem. Phys. 110 (1999) 7650.
[33] J.B. Higgins, R.B. LaPierre, J.L. Schlenker, A.C. Rohrman, J.D. Wood, G.T. Kerr, W.J. Rohrbaugh, Zeolites 8 (1988) 446.
[34] J.M. Newsam, M.M.J. Treacy, W.T. Koetsier, C.B. Gruyter, Proc. Roy. Soc. London A 420 (1988) 375.
[35] C. Baerlocher, W.M. Meier, D.H. Olson, Atlas of Zeolite Structure Types, fifth ed., Elsevier, New York, 2001.
[36] W. Souverijns, W. Verrelst, G. Vanbutsele, J.A. Martens, P.A. Jacobs, J. Chem. Soc., Chem. Commun. (1994) 1671.
[37] L. Lawton, M.E. Leonowicz, R.D. Partridge, P. Chu, M.K. Rubin, Micropor. Mesopor. Mater. 23 (1998) 109.
[38] R. Ravishankar, D. Bhattacharya, N.E. Jacob, S. Sivasanker, Micropor. Mater. 4 (1995) 83.
[39] J.W. Park, S.J. Kim, M. Seo, S.Y. Kim, Y. Sugi, G. Seo, Appl. Catal. A 349 (2008) 76.
[40] M.A. Aramendia, V. Borau, C. Jimenez, J.M. Marinas, R. Roldan, F.J. Romero, F.J. Urbano, Chem. Lett. (2002) 672.
[41] S. Inagaki, K. Kamino, M. Hoshino, E. Kikuchi, M. Matsukata, Bull. Chem. Soc. Jpn. 77 (2004) 1249.
[42] C.M. Tsang, P.-S.E. Dai, F.P. Mertens, R.H. Petty, ACS Petro. Chem. Div. Symp. Prepr. 39 (1994) 367.
[43] A. Platona, W.J. Thomson, Catal. Lett. 101 (2005) 15.
[44] B. Arstad, S. Kolboe, O. Swang, J. Phys. Chem. B 106 (2002) 12722.
[45] W. Song, H. Fu, J.F. Haw, J. Phys. Chem. B 105 (2001) 12839.